Journal of Power Sources 629 (2025) 235833

Contents lists available at ScienceDirect

Journal of Power Sources

journal homepage: www.elsevier.com/locate/jpowsour

Improved chemical durability in polymer electrolyte membranes with nanocellulose-based gas barrier interlayers

I Yang [a], Zulfi Al Rasyid Gautama [b], Yasir Arafat Hutapea [c], Miho Ariyoshi [e], Shigenori Fujikawa [e], Takeharu Sugiyama [f], Stephen Matthew Lyth [c,g,**], Kazunari Sasaki [b,c,d,e], Masamichi Nishihara [a,c,d,e,*]

[a] Graduate School of Integrated Frontier Science, Department of Automotive Science, Kyushu University, 744 Motooka, Nishi-ku, Fukuoka, 819-0395, Japan
[b] Graduate School of Engineering, Department of Hydrogen Energy Systems, Kyushu University, 744 Motooka, Nishi-ku, Fukuoka, 819-0395, Japan
[c] Next-Generation Fuel Cell Research Center (NEXT-FC), Kyushu University, 744 Motooka, Nishi-ku, Fukuoka, 819-0395, Japan
[d] International Research Center for Hydrogen Energy, Kyushu University, 744 Motooka, Nishi-ku, Fukuoka, 819-0395, Japan
[e] International Institute for Carbon-Neutral Energy Research (I^2CNER), Kyushu University, 744 Motooka, Nishi-ku, Fukuoka, 819-0395, Japan
[f] Research Center for Synchrotron Light Applications (RCSLA), Kyushu University, 6-1 Kasuga-koen, Kasuga, Fukuoka, 816-8580, Japan
[g] Department of Chemical and Process Engineering, University of Strathclyde, 75 Montrose Street, Glasgow, G11XL, UK

HIGHLIGHTS

- Fuel cell application of biomaterial cellulose nanocrystals (CNC).
- Multilayered polymer electrolyte membrane (PEM) with a high gas barrier interlayer.
- Gas barrier interlayer made of cellulose nanocrystals (CNC).
- Suppression of radical formation by a gas barrier interlayer.
- Superior chemical durability improvement compared to commercial Nafion.

GRAPHICAL ABSTRACT

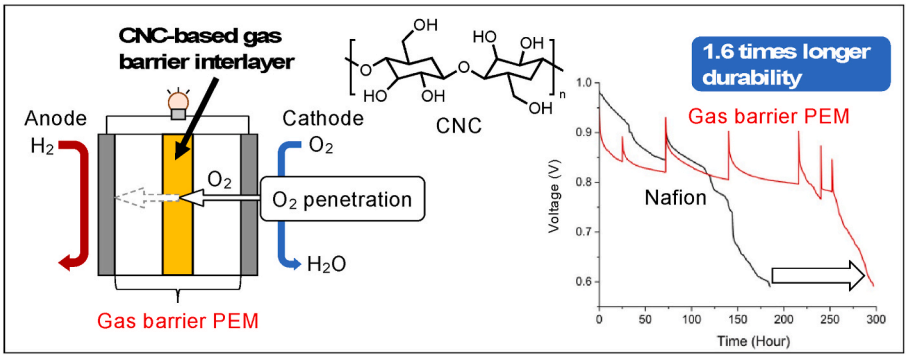

ARTICLE INFO

Keywords:
Polymer electrolyte fuel cells
Polymer electrolyte membranes
Gas barrier property
Chemical durability
Biomaterial
Cellulose nanocrystals

ABSTRACT

Enhancing the lifetime of polymer electrolyte fuel cells (PEFCs) is a key factor in accelerating their application in heavy-duty vehicles (HDVs). A major contributing factor to their worsening performance over time is chemical degradation of the polymer electrolyte membrane (PEM). This is largely caused by the generation of reactive oxygen species such as hydroxyl radicals (•OH) or hydrogen peroxide (H_2O_2), which break down the polymer structure. This radical attack results in a loss of ionic conductivity and thus an increase in cell resistance over the operational lifetime. Here we show that adding an interlayer with suitable gas barrier properties can effectively suppress the generation of reactive oxygen species, slow the rate of membrane thinning, and extend the lifetime

* Corresponding author. Graduate School of Integrated Frontier Science, Department of Automotive Science, Kyushu University, 744 Motooka, Nishi-ku, Fukuoka, 819-0395, Japan.
** Corresponding author. Next-Generation Fuel Cell Research Center (NEXT-FC), Kyushu University, 744 Motooka, Nishi-ku, Fukuoka, 819-0395, Japan.
E-mail addresses: stephen.lyth@strath.ac.uk (S.M. Lyth), nishihara.masamichi.064@m.kyushu-u.ac.jp (M. Nishihara).

https://doi.org/10.1016/j.jpowsour.2024.235833
Received 6 September 2024; Received in revised form 7 November 2024; Accepted 11 November 2024
Available online 5 December 2024

of the cell. We found that cellulose nanocrystals (CNC) blends with poly(vinyl sulfonic acid) (PVS) are suitable composite materials for the interlayer, combining low oxygen permeability with reasonable proton conductivity. Accelerated degradation of the PEMs was investigated via open circuit voltage (OCV) holding tests, in which the device lifetime was reproducibly extended by the incorporation of the CNC/PVS interlayer. Post-mortem analysis revealed that the rate of membrane thinning at the anode side of the PEM after 100 h test was just 30 nm/h, compared with 80 nm/h without an interlayer. Our results clearly confirm that the incorporation of CNC/PVS interlayers with low oxygen permeability into PEMs can suppress chemical degradation and significantly improve the durability of PEFCs. The obtained results also indicate that the concept of the gas barrier PEM for the improved chemical durability of PEMs can be widely and universally applied. We anticipate that this will contribute to the development of next-generation devices with sufficient lifetime for efficient use in fuel cell electric vehicles (FCEVs), including heavy-duty FCEVs.

1. Introduction

Hydrogen-related technologies that can effectively store and convert renewable energy are required to bring about the decarbonization of various industrial sectors [1–4]. In particular, the transition to fuel cell electric vehicles (FCEVs) will significantly contribute to achieving net-zero carbon dioxide emissions targets in the automotive industry [5]. While applications for heavy-duty vehicles (HDVs) are especially anticipated, the requirements for PEFCs in HDVs are more stringent [6]. According to Japan's New Energy and Industrial Technology Development Organization (NEDO) roadmap, the target durability of PEFCs for HDVs needs to increase tenfold to > 50,000 h by 2030 [7]. To achieve this goal, innovative approaches are required to enhance the durability of PEFCs for commercialization.

The degradation of PEFC performance over time is related to the performance drop of the materials consisting of PEFC such as catalysts and polymer electrolyte membranes (PEMs) during the fuel cell operation. In this study, we focused on the PEM issue. PEM is a core component to conduct protons from anode to cathode, insulates against electron conduction to prevent short circuits, and provides a gas barrier of hydrogen and oxygen. At present, sulfonated fluoropolymers such as Nafion or Aquivion are commonly used as PEMs due to their high protonic conductivity and excellent stability in the harsh oxidizing and reducing conditions of a fuel cell [8,9]. However, sulfonated fluoropolymers are classed as per- and polyfluoroalkyl substances (PFAS), which are also known as "forever chemicals" due to their persistence in the environment, and are subject to increasing regulation due to their toxicity to both humans and wildlife [10]. Furthermore, sulfonated fluoropolymers are expensive, contributing significantly to the capital cost of PEFC systems [11–13]. Therefore, as well as supporting the development of decarbonized HDVs, improving the durability will also address the above issues by extending the device lifetime.

The main mode of performance loss in PEMs is chemical degradation. This occurs due to the diffusion of oxygen molecules into the PEMs, where they can form reactive oxygen species (ROS) such as hydrogen peroxide and associated hydroxyl radical species (·OH). These radical species can then break down the polymer structure, resulting in a loss of ionic conductivity. Polymer breakdown is also manifested macroscopically as membrane thinning, eventually leading to pinhole formation. There are three proposed mechanisms for the formation of hydrogen peroxide in PEFCs (Fig. 1, a). The first is the diffusion of oxygen molecules through the PEM from the cathode to the anode, where they then directly react with hydrogen [14,15]. The second is the migration of platinum particles or ions into the PEM from the electrocatalyst layer, which then act as catalyst sites for peroxide formation from oxygen [16]. The third is the generation of hydrogen peroxide at the cathode via 2-electron oxygen reduction, usually catalyzed at transition metal sites arising due to e.g. iron contamination [17,18].

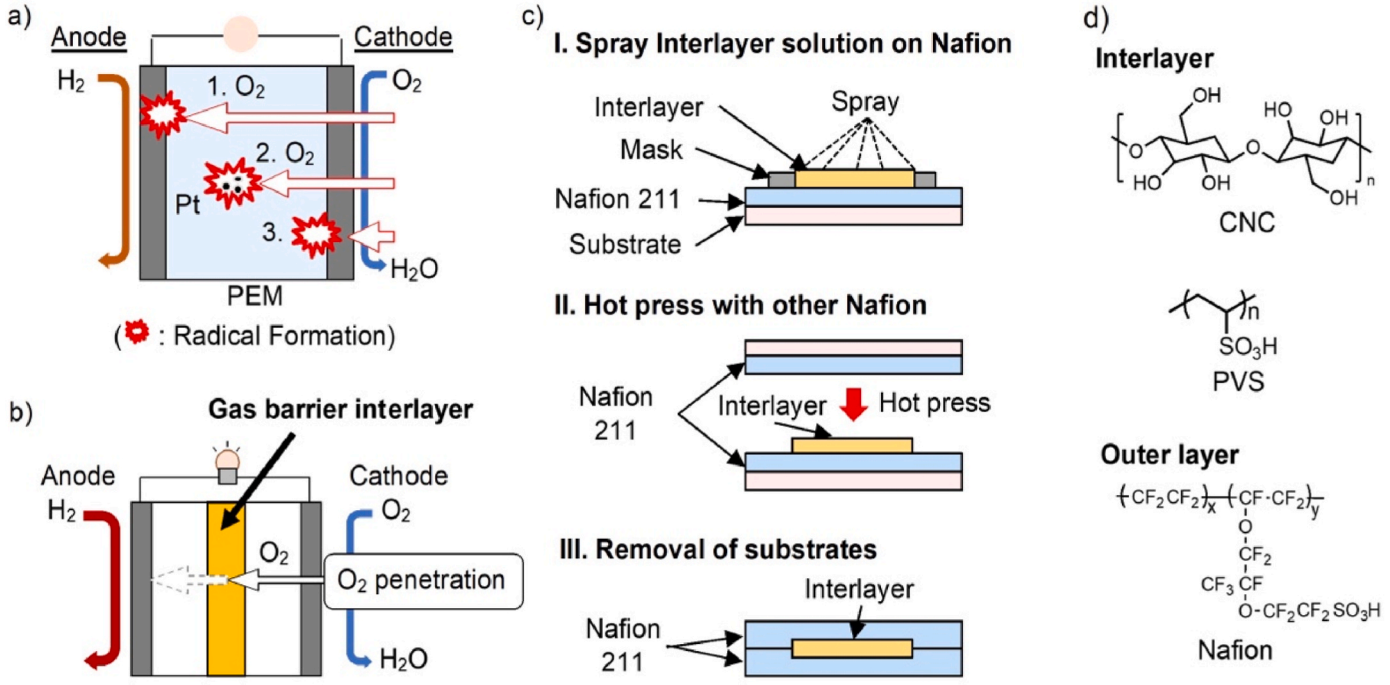

Fig. 1. (a) Three major mechanisms of reactive oxygen species generation during PEFC operation. (b) Schematic diagram showing the function of a gas barrier interlayer in a PEM. (c) Multilayer PEM preparation process via spray deposition, hot pressing, and transfer. (d) Chemical structure of CNC, PVS, and Nafion.

Various methods have already been explored to improve the durability of PEMs against chemical degradation, including the development of alternative hydrocarbon-based polymers with high inherent stability [19–22]. For example, sulfonated poly(phenylene) PEMs have demonstrated superior durability compared to Nafion in open circuit voltage (OCV) holding tests [19,20]. Another method to improve durability is to incorporate radical scavengers such as cerium oxide into polymers, which intercept reactive species before they can damage the polymer [21,22]. Whilst the above methods have resulted in moderate successes, additional approaches are desirable to make further gains in lifetime, towards HDV applications.

In response to this, we have developed an alternative strategy, focusing on the suppression of radical formation in the first place. Gas permeation is a key factor in radical formation, therefore we aim to prevent oxygen diffusion through the PEM. To realize this concept, we explored poly(vinyl alcohol) (PVA) as a general-purpose polymer with excellent gas barrier properties. PVA has lower proton conductivity than Nafion. Therefore, poly(vinyl sulfonic acid) (PVS), known as a proton conductive polymer, was used to improve the proton conductivity as PVA/PVS blends. These two materials are hydrophilic, and not stable in water or humidified conditions. Thus, a free-standing membrane composed solely of the PVA/PVS polymer blend dissolves during PEFC operation. To address this issue, we developed a new material design concept of fabricating multi-layer PEM. Multi-layer PEMs consist of a hydrophilic PVA/PVS interlayer and two water-stable Nafion outer layers to prevent the interlayer dissolution in the humid environment of a PEFC, note as sandwiched PEM in this study. This method successfully resulted in decreased oxygen permeation through the PEM as confirmed in ex situ tests and no delamination occurred in the water uptake test, suggesting that the interlayer was protected [23]. Meanwhile, in OCV holding tests the multilayer PEMs were found to have a significantly extended lifetime (by a factor of 1.7 compared with Nafion 212), attributed to the suppressed radical formation (Fig. 1, b) [23].

To further expand on the concept proven with PVA, we applied cellulose nanocrystals (CNC) as an alternative gas barrier material in this study. Previously, we pioneered the investigation of pure CNC and cellulose nanofibers (CNF) as membrane materials. Cellulose is a fibrous biopolymer material which is generated at a vast scale by plants and bacteria. It is the basis for important goods such as paper, textiles, packaging, food additives, and pharmaceutical products. Nanocellulose can be extracted from cellulosic materials (including waste products) by breaking down the cellulose fibers into smaller dimensions via mechanical or chemical treatments. By their nature, nanocellulose materials are biodegradable, inexpensive, and have minimal environmental impact [24,25]. Nanocellulose has already been applied extensively as a reinforcing additive in PEMs at low concentrations [26,27]. We instead focused on applying pure nanocellulose as a PEM in its own right, demonstrating that the gas permeability of nanocellulose membranes is several orders of magnitude lower than Nafion, and fabricating PEFCs based on CNF and CNC PEMs [25,28]. We also performed sulfonation of CNFs to increase proton conductivity, and deposition of ultrathin membranes to minimize the cell resistance [28]. Furthermore, we investigated crosslinking of CNCs to improve the mechanical properties and durability of cellulose-based PEMs [29].

In related work, we also explored pure graphene oxide as a promising membrane material with extremely low gas permeability, but these were found to have insufficient conductivity or chemical stability for PEFC applications [30–32]. Instead, to take advantage of the excellent gas barrier properties, we sandwiched thin graphene oxide films (~200 nm) between layers of Aquivion, resulting in significantly reduced hydrogen crossover [33]. However, durability tests were not performed.

The utilization of PEMs with inexpensive gas barrier interlayers offers several merits compared to conventional PEM designs. Firstly, the amount of required sulfonated fluoropolymer can be potentially reduced, resulting in lower materials costs and minimizing the reliance on PFAS chemicals. Secondly, the simple preparation method is promising for practical industrial applications, since the multilayer PEMs can be fabricated through additive manufacturing techniques such as spray deposition, simply followed by hot pressing (Fig. 1, c). Thirdly, the preparation process of conventional catalyst-coated membranes (CCM) does not need to be changed or re-optimized, since the outer layers of the PEM are still based on commercial electrolytes such as Nafion [34,35]. As such, fabricating multilayer PEMs with high gas barrier interlayers is a highly promising approach for future PEFC design for FCEV and HDV applications.

In this study, we combine our previous work on gas barrier PEMs and nanocellulose-based PEMs and verify that our material design concept for gas barrier PEMs is available for different gas barrier materials other than PVA. CNC exhibits a low percolation threshold due to its high form factor, which suggests high gas barrier properties [36,37]. Additionally, during the production process of CNC, acid treatment converts some hydroxyl groups into ester-sulfate acid or ester-sulfate salt, which may result in weak proton conductivity [38,39]. However, compared to Nafion, the proton conductivity of CNC is significantly lower [25,28,40]. Therefore, we blended CNC with proton conductive PVS to create a composite electrolyte with high gas barrier properties combined with reasonable ionic conductivity. This blend is then incorporated as an interlayer sandwiched between two commercial Nafion 211 layers and assembled into a PEFC (Fig. 1, d). The PEFC performance and durability are then systematically investigated using accelerated OCV holding tests.

2. Experimental

2.1. PEM fabrication

Cellulous nanocrystal (CNC) powder (CelluForce NCC®, Montreal, QC, Canada) comprises needle-shaped crystals with nominal particle sizes of 7.5 × 150 nm, a specific surface area of 550 m^2/g, a degree of crystallinity of 89.9 %, and a bulk density of 0.7 g/cm^3 [29]. CNC was dispersed in deionized (DI) water and magnetically stirred at 50 °C for at least 24 h to obtain a 10 mg/ml dispersion. Meanwhile, a 25 wt% aqueous solution of the sodium salt of poly(vinyl sulfonic acid) (PVS) was converted to its ionic form via ion exchange in 1M HCl solution for 3 h, using a dialysis membrane (Spectra/Por®6 1kD) with deionized water as a solvent which was regularly replaced until the pH was neutral. The resulting PVS solution was then adjusted to 10 mg/ml. The CNC dispersion and PVS solution were then combined under magnetic stirring in varying ratios of the solids content (100:1, 10:1, and 1:1 wt %).

For membrane preparation (Fig. 1, c), a 3 × 3 cm^2 Nafion 211 (Chemours) substrate was placed onto a hot plate maintained at 65 °C. A poly(ethylene terephthalate) (PET) mask was used to expose a 2 × 2 cm^2 square area of the underlaying substrate. The CNC dispersion, or the CNC/PVS mixtures were loaded into a hand-held spray gun (Tamiya, Spray-work HG), mounted in an auto spray machine with a controllable moving stage (C-3 J, Nordson K.K.), and connected to an air compressor (HG air compressor, Revo II, Tamiya). The mass of the sprayed material was tracked by placing carbon gas diffusion layers (GDL, EC-TP1-060T, Toray) with an area of 1 × 1 cm^2 on the PET mask on either side of the target area, which could be removed and weighed. Using this method, the error in mass calculations was kept to within ±3 wt%. After spraying a suitable amount of CNC/PVS material onto the Nafion 211 surface, the mask was removed and a second layer of Nafion 211 placed over the top. This multilayer structure was then hot-pressed at 140 °C and 0.3 kPa for 5 min (Digital Press CYPT-10, Sinto). A double-layer reference PEM with no interlayer was also prepared by simply placing two Nafion 211 membranes together and hot pressing under the same conditions (noted as Nafion 211DL in this study). Furthermore, free-standing CNC and CNC/PVS membranes with the same mass ratios were fabricated by casting. In this case the prepared CNC/PVS solutions were cast into polytetrafluoroethylene (PTFE) petri dishes (Sigma Aldrich) and dried at

40 °C for 24 h before being removed and stored in sealed bags to prevent moisture ingress. The sample names of the resulting PEMs investigated in this study are summarized in Table 1.

2.2. PEM characterization

The resulting PEMs were characterized via X-ray diffraction with Cu Ka (1.54 Å) (SmartLab 9 kW AMK X-ray Diffractometer, Rigaku), proton conductivity measurements (MTS-740, Scribner associates Incorporation and SI-1260, Solartron), gas permeability tests (GTR-11A/31A gas permeability tester, GTR TEC Corporation), as reported in our previous works [23]. Descriptions of dimensional stability, water uptake, and wide-angle X-ray scattering (WAXS) can be found in the Supporting Information.

2.3. Membrane electrode assembly (MEA) fabrication and cell assembly

Electrocatalyst ink was prepared by combining 120 mg of platinum-decorated ketjen black (Pt-KB, 46.8 wt%, TEC10E50E, Tanaka Kikinzoku Kogyo K.K.), 0.952 mL of 5 wt% Nafion dispersion (FUJIFLIM Wako Pure Chemicals Corporation), 5.699 mL of ethanol (FUJIFLIM Wako Pure Chemicals Corporation) and 0.570 mL of DI water and homogenizing in ice bath for 30 min via ultrasonication (NR-50M, Microtech CO). The obtained electrocatalyst ink yields to 28 wt% of Nafion ionomer in the electrocatalyst layer [23]. This was quickly loaded into the reservoir of an auto-spray machine (C-3 J, Nordson K.K.). Catalyst coated membranes (CCM) were then fabricated by placing the PEM on a controllable hot stage at 65 °C, covering with a PET mask leaving an area of 1x1 cm^2. To track the deposited mass to within ±3 wt %, a 1 × 1 cm^2 GDL was placed on either side of the target, which could be removed and weighed. The target loading on both sides of the PEM was 0.3 mg_{Pt}/cm^2. After catalyst deposition, the coated PEM was hot-pressed at 132 °C and 0.3 MPa for 180 s (Digital Press CYPT-10, Sinto). Membrane electrode assemblies (MEAs) were then prepared by sandwiching the PEM between two GDLs (EC-TP1-060T, Toray). These were then placed into a Japan Automotive Research Institute (JARI) cell holder with a 1 cm^2 electrode area, and this was tightened to 0.4 N m using a torque wrench (QL5N-MH, Tohnichi).

Table 1
Summary of the sandwich PEMs investigated in this study.

Sample name	Weight ratio (CNC:PVS)	Areal density of interlayer (mg/cm^2)	Total thickness (μm)
Nafion Reference Membranes			
Nafion 212	–	–	50
Nafion 211	–	–	25
Nafion 211DL	–	–	50
CNC/PVS Membranes			
CNC	–	–	28.6
R1	1:1	–	33.4
R10	10:1	–	26.8
R100	100:1	–	31.2
Nafion | CNC | Nafion Sandwich Membranes			
CNC-0.25 mg	–	0.25	51.7
CNC-0.5 mg	–	0.5	53.4
CNC-1mg	–	1.0	55.2
Nafion | CNC/PVS | Nafion Sandwich Membranes			
R1-1 mg	1:1	1.0	55.5
R10-1 mg	10:1	1.0	55.4
R100-1 mg	100:1	1.0	55.3

2.4. PEFC performance evaluation

Fuel cell tests were conducted at 80 °C and 95 % RH, using a fuel cell test station (AUTOPEM-CVZ01, Toyo Corporation) connected to an electrochemical interface system and impedance analyzer (SI-1287, SI-1255B, Solartron). Before measuring fuel cell performance, 3 h aging process at 0.6 V was carried out under hydrogen gas flow (139 ml/min) at the anode and air flow (332 ml/min) at the cathode. Under the same test setting, polarization curves (IV curves) and impedance spectroscopy were carried out, IV curves were obtained by sweeping the potential from the OCV to 0.2 V, at a scan rate of 20 mV/s, and impedance spectra were also recorded by varying the frequencies from 10 to 100,000 Hz, at current values of 0.05, 0.1, 0.2, 0.4, and 0.6 A. Hydrogen crossover current density (HCCD) was obtained by then changing the gases at the anode and cathode to 70 ml/min hydrogen, and 166 ml/min nitrogen, respectively, and the potential was swept from 0.2 V to 0.5 V at 5 mV/s. Finally, the gas flow at the cathode was stopped and the gas flow at the anode was maintained at 70 ml/min, and cyclic voltammograms (CV) were obtained by cycling between 0.05 V and 0.9 V at 50 mV/s. Descriptions of the calculation from electrochemical surface area (ECSA) from CV spectra can be found in the Supporting Information.

2.5. Accelerated durability tests

Chemical durability was evaluated using open circuit voltage (OCV) holding tests. The cell was maintained at 90 °C and 30 % RH, with hydrogen gas flow of 139 mL/min at the anode, and an air flow of 332 mL/min at the cathode. At regular intervals of 72 h the cell conditions or significant voltage drop happening were changed to 80 °C and 95 % RH for fuel cell evaluation as described above. The cell conditions were then returned to 90 °C and 30 % RH to continue the OCV holding test. The end-of-life of the cell was defined at the point at which the OCV dropped to 0.6 V, at which point the measurement was stopped for safety reasons.

Post-mortem analysis was performed after aging the cells, after 100 h, and at end-of-life. The cell holder was disassembled, and the MEA removed. For the cross-section image of the samples, the MEA was cut and filled with cold setting epoxy resin (NER-814M, NISSHIN EM Corporation)/epoxy resin hardner (NER-814B, NISSHIN EM Corporation) mixture, which ratio of resin to hardner was 3 to 1 (vol.), by using the flexible rubber mold (TAAB Laboratories Equipment Corporation), then dried at room temperature (25 °C) for at least 3 days. After drying process, the solid resin samples were cut by using microtome (EM UC6, Leica) and coated with gold under 5 Pa pressure and 0.8 V for 3 min (SC-701 MkII ECO, Sanyu Electron). The prepared samples were observed via scanning electron microscopy (FIB/SEM Dual Beam Versa3D LoVac, FEI Company Japan Ltd.), and elemental mapping performed via energy dispersive spectroscopy (EDS) (FIB/SEM Dual Beam Versa3D LoVac, FEI Company Japan Ltd.).

3. Results and discussions

3.1. The effect of sandwich structure for PEMs

In this study, high gas barrier CNC and proton conductivity enhancer PVS were used. Since these two materials are hydrophilic, free-standing membranes are not suitable for PEFC operation conditions. CNC membranes that have not undergone crosslinking or hydrophobization easily swell, rupture, and disperse in water. Similarly, PVS dissolves in water. This would be detrimental in the humid environment of a PEFC. Instead, choosing the sandwiched fabrication, in which a CNC/PVS blend interlayer is sandwiched between two water-stable Nafion 211 layers as the multilayer membranes, noted as sandwiched PEM, expected to be stable in humified condition or aqueous media. This method has been proved in our previous study [23]. For these reasons, the sandwiched PEMs of CNC/PVS blend interlayer were prepared by the method mentioned above, and the sandwiched PEM without an interlayer,

Nafion 211 double layers (Nafion 211DL), was also prepared as the reference.

To confirm whether the sandwiched PEMs stabilize in the humified condition of a PEFC, we performed water uptake test as the preliminary test to understand the effect of sandwich structure on PEMs (Table S-1 and S-2). The membranes were first immersed in water at room temperature for 24 h. After that, it was confirmed visually that no delamination occurred, suggesting that the water-soluble interlayer was protected from water by two Nafion outer layers. The overall increase in water uptake as the ratio of CNC in the CNC/PVS interlayer increased

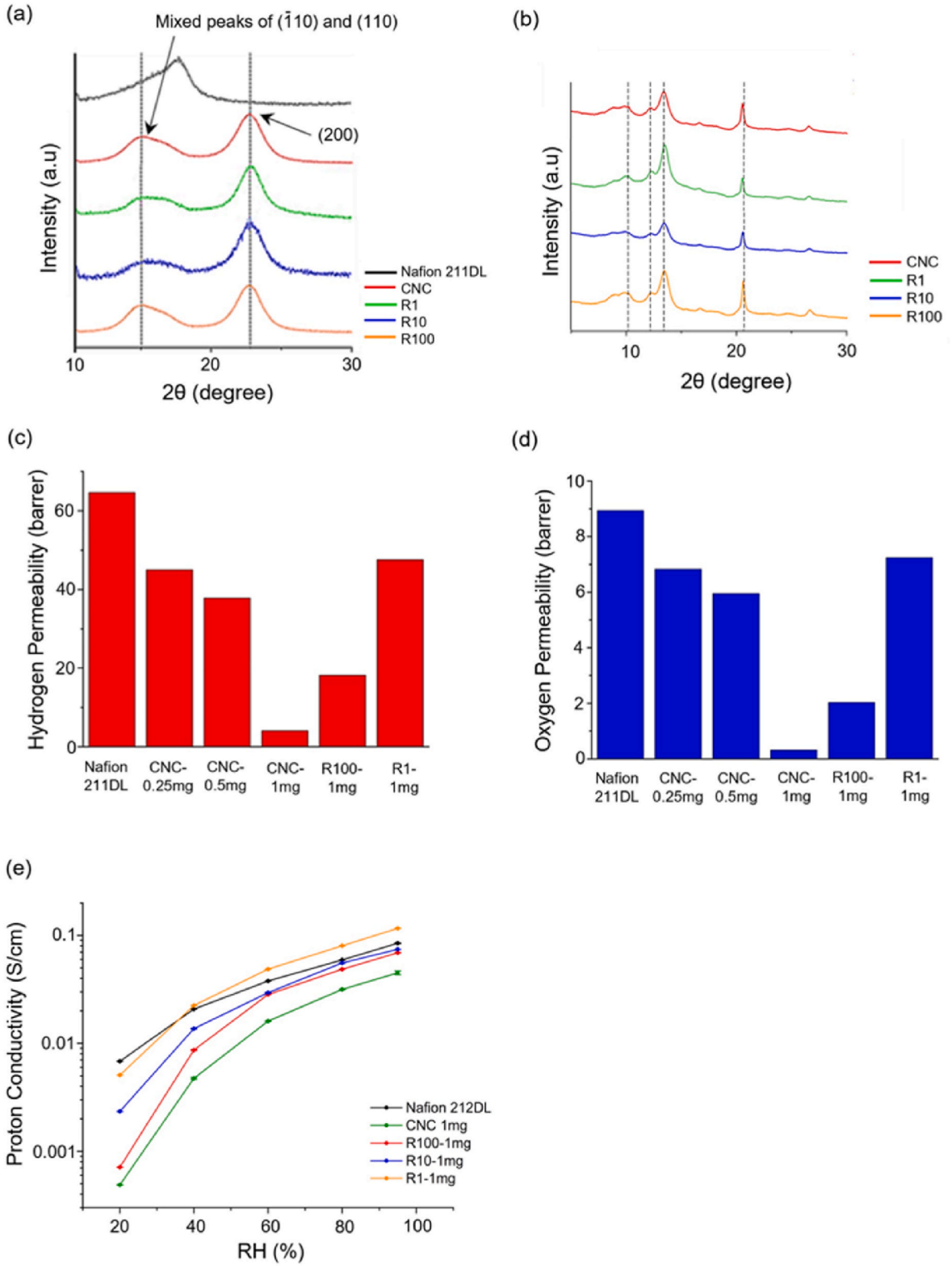

Fig. 2. (a) XRD patterns of Nafion 211DL and the free-standing membranes. WAXS patterns of (b) humidified condition of CNC, R1, R10 and R100. Gas permeability measurements at 80 °C under dry conditions: (c) hydrogen and (d) oxygen. (e) Proton conductivity of Nafion 211DL and multilayer PEM with various CNC/PVS ratios measured at 80 °C under different values of relative humidity.

from 1 to 100 reflects the hydrophilic natures of the interlayer materials. Areal swelling (i.e. the relative change in diameter) was negligible for all samples. On the other hand, there was a significant relative increase in thickness change, compared to Nafion 211DL. These results indicate that the outer Nafion layers help to restrict swelling in-plane but have little impact on through-plane swelling. This is as expected given the geometry of the multilayer PEMs. As above preliminary test, the concept of sandwich structure for PEMs was confirmed that they were stable in water without delamination behavior, expected to be stable in the humid condition of a PEFC.

3.2. Molecular structure

XRD was performed on free-standing CNC/PVS membranes to evaluate the effect of relative proportions on the structure (Fig. 2a). Nafion 211DL displays a major peak at ~17°, corresponding to an average interchain distance of 0.52 nm [41]. CNC and CNC/PVS display major peaks at 15° (d = 0.59 nm) and 22.5° (d = 0.40 nm), corresponding well with overlapping $(1\bar{1}0)$, (110) and (200) crystallographic planes previously reported for CNC [42]. The peak at 22.5° is attributed to hydrogen bonding between adjacent hydroxyl groups in CNC, and it has been reported that the polymer chains in CNC are tightly packed and stabilized by a strong hydrogen-bonding network [42]. This close-packed crystalline structure provides an explanation for observed low gas permeability of CNC membranes relative to Nafion. Meanwhile, it has previously been reported that the sulfonic acid groups of PVS can disrupt the crystalline structure of CNC [43], but in this case no trend is observed with PVS ratio.

Furthermore, the WAXS profile of Nafion 211DL (Figs. S–1a) displays two major peaks at ~1.17 $Å^{-1}$ and 2.70 $Å^{-1}$, corresponding to an amorphous peak and a superimposed crystalline peak, respectively [44]. No change is observed between dry and wet conditions, suggesting that these peaks are not related to the hydrophilic domains formed by the sulfonic acid group [41,45]. Meanwhile, CNC and CNC/PVS (Figs. S–1b), have major peaks at corresponding to the $(1\bar{1}0)$ and (110) planes of CNC (1.17 $Å^{-1}$), the (200) plane of CNC (1.41 $Å^{-1}$), the (040) plane of CNC (1.59 $Å^{-1}$), and, the (102) plane (2.40 $Å^{-1}$), respectively [46–48]. Again, no significant changes are observed between the dry and wet states (Fig. 2b).

3.3. Gas permeability

The main objective of introducing an interlayer into the PEM in this work is to reduce the gas permeability and thereby suppress peroxide formation and radical attack. Here, the hydrogen and oxygen gas permeabilities are evaluated under dry conditions at 80 °C (Fig. 2c and d). For Nafion 211DL, the H_2 and O_2 gas permeabilities are 64.6 and 8.9 barrer, respectively. Introducing the interlayer decreases the permeability in all cases. Increasing the thickness of the interlayer (i.e. increasing the areal mass density) results in a corresponding decrease in permeability, with the thickest interlayer reducing the permeability by around an order of magnitude to values of 4.1 and 0.3 barrer, respectively. Meanwhile, increasing the PVS content of the interlayer significantly increases the permeability, with a 1:1 ratio corresponding to permeabilities of 49 and 7.3 barrer, respectively. This is attributed disruption of the hydrogen bond network in CNC due to interactions with the sulfonic acid groups of PVS, or alternatively simply because PVS has higher permeability compared with CNC. This result showed the same trend as observed with the PVA-based gas barrier PEM [23]. Overall, these results clearly confirm that the inclusion of CNC or CNC/PVS interlayers in Nafion PEMs significantly reduces both hydrogen and oxygen gas permeability.

3.4. Proton conductivity

Whilst the gas permeability has been confirmed to decrease when adding an interlayer, the proton conductivity must also be sufficient to allow for reasonable PEFC performance. We have previously shown that CNC is a proton conductor, but the hydroxyl groups of CNC are weakly acidic, limiting their effectiveness for ion transport, and resulting in relatively low proton conductivity [25]. This can be compensated by reducing the thickness of the interlayer, or by blending with a high-conductivity material (such as PVS). Fig. 2e shows the proton conductivity for PEMs with different CNC/PVS ratios measured at 80 °C and a range of RH values. Nafion 212DL has a maximum conductivity of 85 mS/cm, which is comparable to reported values [9]. Adding a CNC interlayer significantly decreases the proton conductivity (~43 mS/cm at 95 % RH), due to the relatively low conductivity of CNC itself. Adding a CNC/PVS blend interlayer increases the proton conductivity in proportion to the amount of PVS. Interestingly, the highest proportion (CNC/PVS = 1:1) results in even higher conductivity than Nafion 212DL. The reasons for this are not immediately clear, but the addition of PVS may assist with lowering the contact resistance between the two Nafion layers. These measurements clearly confirm that CNC/PVS blends are highly suited to be used as interlayers in Nafion PEMs without compromising the conductivity.

3.5. Fuel cell performance

From the results of gas permeability and proton conductivity, when CNC increases in the interlayer, gas barrier property can be improved, but proton conductivity deceases at the same time. Therefore, considering the balance of gas barrier property and proton conductivity, we selected R100-1 mg as a PEM for fuel cell performance and durability test since 1 mg/cm^2 areal loading amount has better gas barrier property than 0.25 and 0.5 mg/cm^2 areal loading, and CNC:PVS = 100:1 (note as R100) can show proton conductivity in blend interlayer without losing gas barrier property so much.

The resulting gas barrier PEMs were incorporated into MEAs and assembled into a cell holder for PEFC testing at 80 °C and 95 % RH (Figs. S–2 and Fig. 3). For Nafion 211DL, the results are comparable with those reported in the literature for similar thickness under similar conditions. The slightly lower performance can be attributed to the interfacial resistance between the two Nafion layers. For pure CNC interlayers the performance drops considerably (Figs. S–2a). This is attributed to the relatively low proton conductivity of CNC compared with Nafion, and this is confirmed by the slope of the I-V curve in the ohmic region, and by impedance measurements (Figs. S–2a). However, a clear trend of improving performance with decreasing thickness is observed. The hydrogen crossover current density is much lower when adding a CNC interlayer (Figs. S–2c), confirming the gas barrier properties of the interlayer. However, a relatively low OCV is observed, which is attributed to lower ECSA (Figs. S–2d). This is discussed further below.

Meanwhile, adding CNC/PVS interlayers still results in lower overall performance than Nafion 221 DL. However, there is a clear trend in increasing performance as the PVS ratio increases (Fig. 3a). For the highest PVS content (CNC: PVS = 1:1) a similar slope is observed in the ohmic region compared with Nafion 221 DL. Similar membrane resistance is obtained by impedance spectroscopy (Fig. 3b). This shows that blending PVS with CNC has a significant impact on proton conductivity. Furthermore, the PEMs with CNC/PVS interlayers have significantly lower hydrogen crossover compared with Nafion 221 DL (Fig. 3c), confirming that the gas barrier properties are retained, despite blending with PVS.

Again, the OCV is lower than the case of Nafion 221 DL, which presents a significant challenge for gas barrier PEMs. Since the hydrogen crossover current is lower (Fig. 3c), this is attributed to lower electrochemically active surface area (ECSA) (Fig. 3d). We propose that the

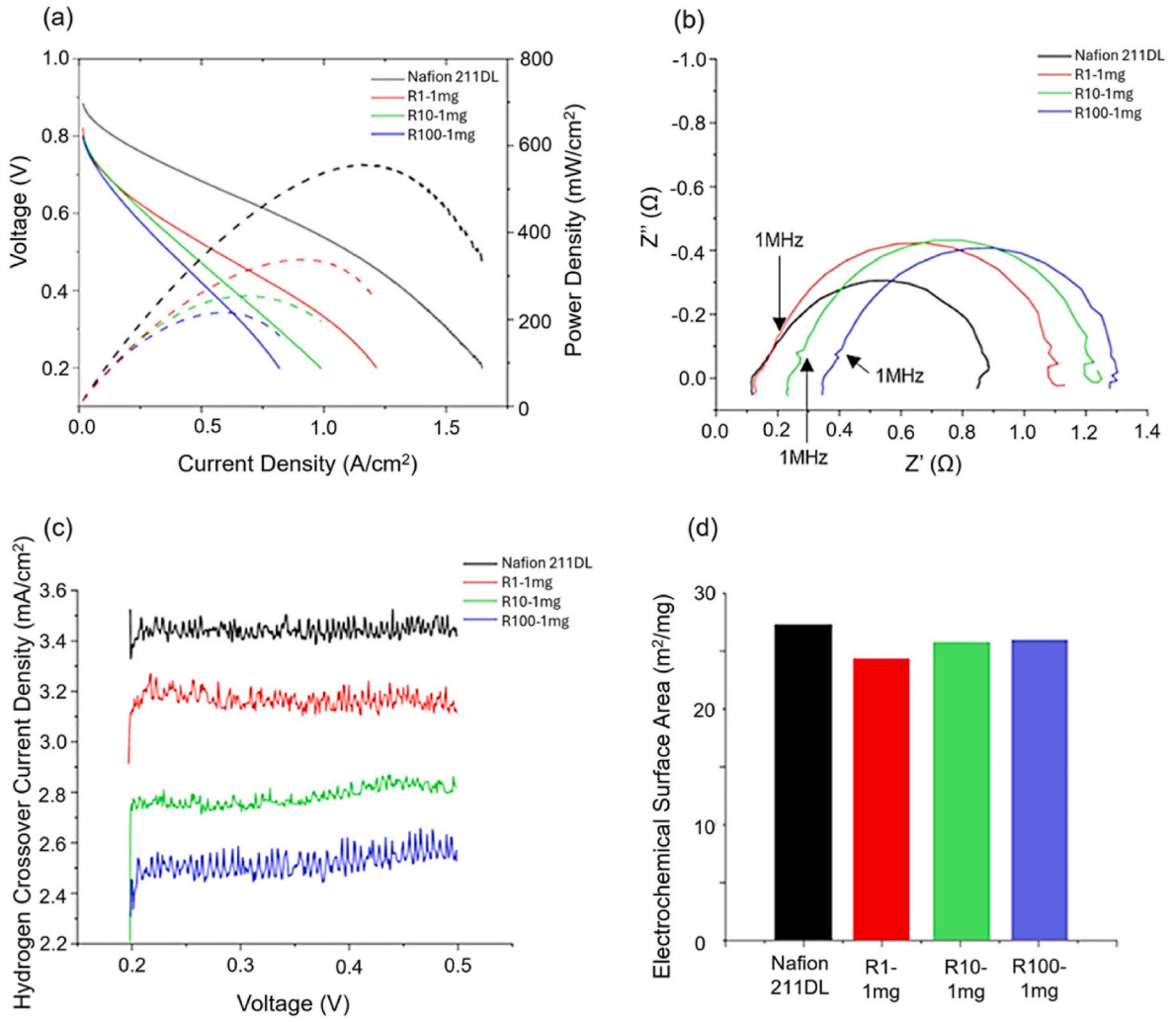

Fig. 3. Performance of PEFCs fabricated using Nafion 211DL and CNC/PVS interlayers with varying ratios, measured at 80 °C and 95 % relative humidity: (a) I-V curves, (b) impedance spectra, (c) hydrogen crossover current density, and (d) ECSA results.

lower ECSA is due to poisoning of the Pt catalyst due to leaching of the decomposed sulfuric acid from PVS during MEA preparation at 132 °C [49–51]. In addition, there is a possibility that a small amount of sulfonic acid may leach from the CNC. Current mass production of CNC generally uses sulfuric acid, leading to a partial esterification of the hydroxyl function groups on CNC, forming a strong ester-sulfate acid [1,2,52–54]. The ester-sulfate acid could easily decompose into sulfuric acid again by aqueous acidic hydrolysis in fuel cell operation, and decomposed sulfuric acid may poison the Pt catalyst, leading to less active Pt in the catalyst layer, resulting in lower ECSA performance and lower OCV. To investigate this further, the duration of the PEFC conditioning step was varied (Figs. S–3). A clear improvement in I-V performance is observed when the conditioning step is increased from 3 to 12 h, and this is attributed to the removal of sulfur-based adsorbents from the platinum surface.

3.6. Accelerated durability tests

Based on the above results, a PEFC was assembled using a gas barrier PEM with a CNC/PVS interlayer at a ratio of 100:1, and an areal density of 1.0 mg/cm^2 for OCV holding tests (Fig. 4a). This choice was made because of the balance between reasonable initial I-V performance and the need for low gas permeability, to test our hypothesis that a gas barrier interlayer will improve the chemical durability. The OCV holding test is an accelerated stress test conducted at 90 °C and 30 % RH. A PEFC using a Nafion 211DL PEM survived for 184 h before end-of-life was reached (i.e. the potential dropped to <0.6 V). The average voltage dropped over the first 125 h was 1.54 mV/h, and then a much rapid drop was observed, indicating membrane failure. Meanwhile, the PEFC fabricated using a CNC/PVS interlayer survived for a much longer time. In this case, a much lower average voltage drop of 0.66 mV/h was recorded up until 252 h, followed by a similar rapid voltage drop until end-of-life at 295 h. A second test was also performed and end-of-life values of 183 and 292 h were obtained (Figs. S–4), respectably, confirming reproducibility. Meanwhile, for Nafion 211DL, the hydrogen crossover current density increased from 3.1 mA/cm^2 at the beginning of the test to a very large value of 392.2 mA/cm^2 after 184 h (Fig. 4c and d). In contrast, the CNC/PVS interlayer resulted in lower initial hydrogen crossover (2.4 mA/cm^2), which increased at a slower rate, finally reaching 178.0 mA/cm^2 after 295 h (Fig. 4c and d). This confirms that incorporating a CNC/PVS interlayer suppresses hydrogen crossover, even under harsh accelerated testing conditions.

The cell resistance was also determined at regular intervals (72 h) throughout the OCV holding test via impedance measurements (Fig. 4b). For Nafion 211DL, the cell resistance increased at a relatively constant rate throughout the measurement, attributed to conventional chemical degradation by reactive oxygen species, resulting in a loss of ionic conductivity. In stark contrast, for the CNC/PVS interlayer, the cell resistance undergoes an unexpected decrease during the first part of the test, before increasing as expected until end-of-life. This bell-shaped

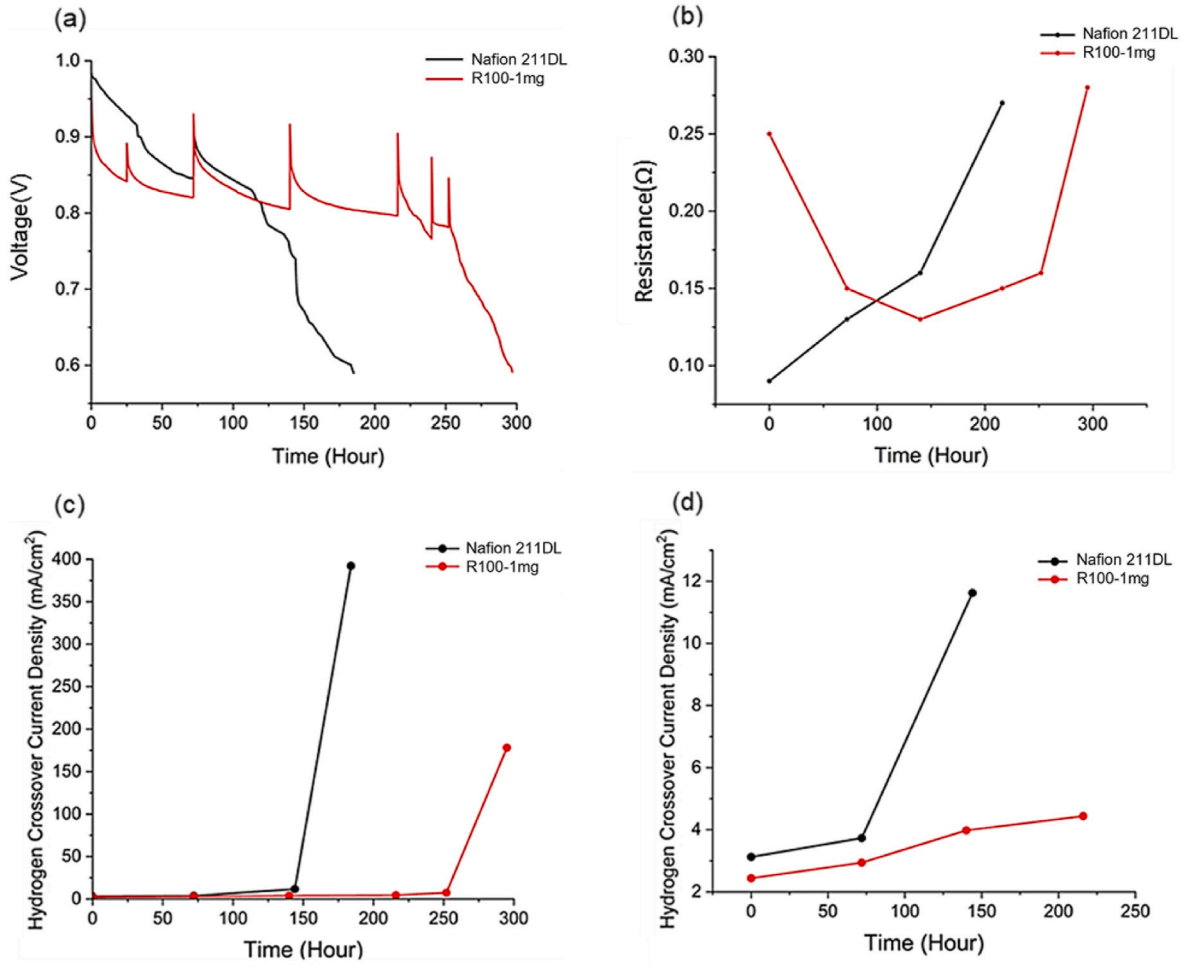

Fig. 4. OCV holding test results for Nafion 211DL and Nafion 211 with a CNC/PVS interlayer. (a) Cell potential, (b) cell resistance, (c) hydrogen crossover current density, and (d) enlarged region of the hydrogen crossover current density data.

change of the resistance would be related to membrane thinning and chemical degradation of the sulfonic acid group in the membrane from radical attacks. First, the cell resistance decreases due to membrane thinning caused by radical attacks, especially the anode side Nafion layer. Subsequently, the increase in resistance due to the decomposition of sulfonic acid would be more prominent than the decrease in resistance caused by membrane thinning, resulting in a bell-shaped change. We consider that this behavior is changed by the change of experimental or material conditions, such as the composition, thickness, and gas barrier properties of the interlayer, etc. [23].

3.7. Post-mortem characterization

Finally, SEM and EDS observation was performed on MEA cross-sections before and after OCV holding tests. For Nafion 211DL, the initial thickness of the PEM is 50 μm, corresponding to two Nafion 211 layers (Fig. 5a). After compression and 3 h of cell conditioning, no difference is observed (Fig. 5b). After 100 h of the OCV holding test, the anode-side Nafion 211 layer decreased significantly to 17 μm whilst the cathode-side layer decreased slightly to 22 μm (Fig. 5c). This corresponds to thinning rates of 80 nm/h at the anode, and 30 nm/h at the cathode. At end-of-life, the anode-side Nafion layer is just 4 μm and the cathode-side layer is 18 μm (Fig. 5d). These results show that Nafion undergoes severe thinning during OCV holding tests, as has been reported in numerous previous studies [18,23,55,56]. Furthermore, it clearly shows that thinning occurs predominantly at the anode side of the membrane by OCV holding test.

Meanwhile, for MEAs incorporating a CNC/PVS interlayer, the total thickness of the PEM after fabrication is ~55 μm (Fig. 5e). This is slightly thicker than Nafion 211DL due to the added thickness of the interlayer (5.1 μm). The interlayer decreases to 3.8 μm after the cell assembly with compression and a 3-h aging process, while the thicknesses of the Nafion do not change (Fig. 5f). After 100 h, the total thickness of the cell is reduced to 45 μm (Fig. 5g), corresponding to an interlayer thickness of 1.9 μm, an anode-side Nafion thicknesses of 22 μm, and a cathode-side Nafion thickness of 23 μm. The corresponding Nafion 211 thinning rates are 30 nm/h at the anode and 20 nm/h at the cathode, both values being slower compared with the Nafion 211DL PEM, especially at anode-side Nafion. Finally, at end-of-life, the total thickness decreases to 24 μm, corresponding an anode-side Nafion thicknesses of 7 μm and a cathode-side thickness of 17 μm (Fig. 5h). The interlayer is too thin for the thickness to be clearly determined from SEM images, and EDS images (Figs. S–5) suggest that the interlayer is no longer continuous.

These post-mortem results confirm that the addition of a CNC/PVS interlayer significantly reduces the rate of membrane during OCV holding tests, in agreement with the electrochemical data. The interlayer itself also clearly undergoes thinning from the beginning of the test, providing further explanation for the initial decrease in cell resistance observed in impedance measurements. Eventually, the interlayer is largely consumed and is longer effective as a gas barrier. At this point the rate of thinning of the Nafion layers increases as they are exposed to reactive oxygen species and undergo conventional chemical degradation until end-of-life. It should be noted that the number of hours taken to reach end-of-life is much longer than for the Nafion 211DL PEM, which

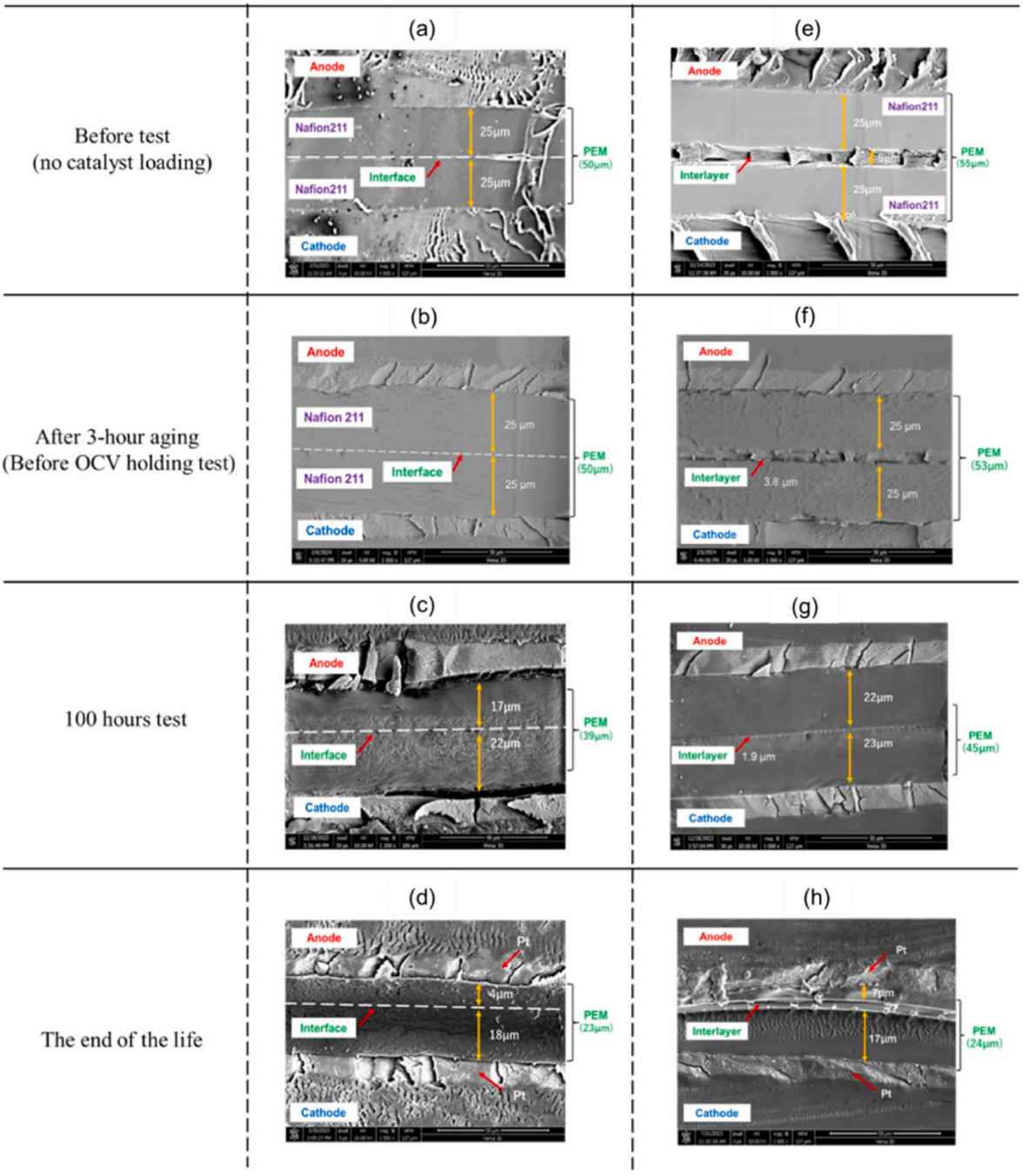

Fig. 5. SEM observation of MEA cross-sections taken at various points throughout OCV holding tests: (a)–(d) Nafion 211DL, and (e)–(h) R100-1 mg.

is why the final states of both cells look similar in SEM images.

4. Conclusions

In this study, we investigated the suppression of chemical degradation of PEMs by the incorporation of CNC/PVS interlayers with high gas barrier properties. Ex-situ measurements confirmed that adding an interlayer significantly decreased the gas permeability, without significantly compromising the proton conductivity, and the effect of interlayer thickness and composition was also investigated. PEFCs were fabricated using an interlayer with a CNC/PVS ratio of 100:1 and an areal density of 1 mg/cm^2 (~5 μm), sandwiched between two commercial Nafion 211 membranes. In OCV holding tests the incorporation of the interlayer extended the cell lifetime by a factor of 1.6 times compared to a double layer of Nafion 211 with no interlayer. Post-mortem analysis revealed that the rate of thinning was significantly slower in the interlayer-containing PEMs. This work confirmed that incorporating CNC/PVS interlayers with high gas barrier properties in PEMs suppresses the generation of reactive oxygen species, significantly improving durability. Although some challenges remain in the application of such multilayer PEMs in real-world systems, the results of this study are expected to have significant implications for the development of next-generation PEFCs. Additionally, the results of this study demonstrate that the concept of gas barrier PEMs can be widely and universally applied to various materials. The observed improvements in durability are especially relevant to heavy-duty fuel cell electric vehicles, in which durability is particularly important.

CRediT authorship contribution statement

I Yang: Writing – original draft, Validation, Methodology, Investigation, Funding acquisition, Formal analysis, Data curation, Conceptualization. **Zulfi Al Rasyid Gautama:** Writing – review & editing, Investigation. **Yasir Arafat Hutapea:** Writing – review & editing, Methodology, Investigation. **Miho Ariyoshi:** Data curation. **Shigenori Fujikawa:** Writing – review & editing, Resources, Data curation. **Takeharu Sugiyama:** Writing – review & editing, Resources, Funding acquisition, Formal analysis, Data curation. **Stephen Matthew Lyth:** Writing – review & editing, Supervision, Resources, Investigation, Funding acquisition, Conceptualization. **Kazunari Sasaki:** Writing – review & editing, Resources, Conceptualization. **Masamichi Nishihara:** Writing – review & editing, Writing – original draft, Visualization, Supervision, Resources, Project administration, Methodology, Investigation, Conceptualization.

Declaration of competing interest

The authors declare the following financial interests/personal relationships which may be considered as potential competing interests:

Masamichi Nishihara reports financial support was provided by JSPS. Stephen M. Lyth reports financial support was provided by RSC. If there are other authors, they declare that they have no known competing financial interests or personal relationships that could have appeared to influence the work reported in this paper.

Acknowledgements

The authors gratefully acknowledge financial support by JSPS KAKENHI Grant Number JP23K04419, an RSC Researcher Collaboration Grant (C23-1081885414), and the Toyota Mobility Foundation 2019. SAXS experiments were performed on Kyushu University Beamline at Saga Light Source (SAGA-LS/BL06, proposal No. 2023IIK003).

Appendix A. Supplementary data

Supplementary data to this article can be found online at https://doi.org/10.1016/j.jpowsour.2024.235833.

Data availability

Data will be made available on request.

References

[1] A.L. Chibac-Scutaru, S. Coseri, Advances in the use of cellulose-based proton exchange membranes in fuel cell technology: a review, Int. J. Biol. Macromol. 247 (2023) 125810, https://doi.org/10.1016/j.ijbiomac.2023.125810.
[2] R. Calle-Gil, E. Castillo-Martínez, J. Carretero-González, Cellulose nanocrystals in sustainable energy systems, Adv. Sustainable Syst. 6 (2022) 2100395, https://doi.org/10.1002/adsu.202100395.
[3] M. Asandulesa, A.L. Chibac-Scutaru, M.E. Culica, V. Melinte, S. Coseri, Cellulose-based films with enhanced load of nitrogen containing heterocycles: the impact on the surface morphology and proton conductivity, Appl. Surf. Sci. 607 (2023) 1550771, https://doi.org/10.1016/j.apsusc.2022.155077.
[4] K. Sasaki, H.-W. Li, A. H, et al., Hydrogen Energy Engineering: A Japanese Perspective, Wiley, Japan, 2016, https://doi.org/10.1007/978-4-431-56042-5.
[5] Reducing CO_2 emissions from heavy-duty vehicles, Climate Action, European Commission. https://climate.ec.europa.eu/eu-action/transport/road-transport-reducing-co2-emissions-vehicles/reducing-co2-emissions-heavy-duty-vehicles_en.
[6] IEC, Net Zero by 2050, A Roadmap for the Global Energy Sector, p.135. https://iea.blob.core.windows.net/assets/deebef5d-0c34-4539-9d0c-10b13d840027/NetZeroby2050-ARoadmapfortheGlobalEnergySector_CORR.pdf.
[7] Japan Government, NEDO hydrogen roadmap (in Japanese), https://www.nedo.go.jp/library/battery_hydrogen.html, 2023.
[8] F. Xiao, Y. Wang, Z. Wu, G. Chen, F. Yang, S. Zhu, K. Siddharth, Z. Kong, A. Lu, J. Li, C. Zhong, Z. Zhou, M. Shao, Recent advances in electrocatalysts for proton exchange membrane fuel cells and alkaline membrane fuel cells, Adv. Mater. 33 (2021) 2006292, https://doi.org/10.1002/adma.202006292.
[9] L. Liu, W. Chen, Y. Li, An overview of the proton conductivity of nafion membranes through a statistical analysis, J. Membr. Sci. 504 (2016) 1–9, https://doi.org/10.1016/j.memsci.2015.12.065.
[10] E.C. Agency, Regulation of Per- and polyfluoroalkyl substances (PFAS). https://echa.europa.eu/hot-topics/perfluoroalkyl-chemicals-pfas, 2023.
[11] T. Ishimoto, M. Koyama, A review of molecular-level mechanism of membrane degradation in the polymer electrolyte fuel cell, Membranes 2 (2012) 395–414, https://doi.org/10.3390/membranes2030395.
[12] P.C. Okonkwo, I. BenBelgacem, W. Emori, P.C. Uzoma, Nafion degradation mechanisms in proton exchange membrane fuel cell (PEMFC) system: a review, Int. J. Hydrogen Energy 46 (2021) 27956–27973, https://doi.org/10.1016/j.ijhydene.2021.06.032.
[13] Chemrous, Commercial cost of Nafion, https://www.nafion.com/en.
[14] V.A. Sethuraman, J.W. Weidner, A.T. Haug, S. Motupally, L.V. Protsailo, Hydrogen peroxide formation rates in a PEMFC anode and cathode, J. Electrochem. Soc. 155 (2008) B50–B57, https://doi.org/10.1149/1.2801980.
[15] M. Inaba, T. Kinumoto, M. Kiriake, R. Umebayashi, A. Tasaka, Z. Ogumi, Gas crossover and membrane degradation in polymer electrolyte fuel cells, Electrochim. Acta 51 (2006) 5746–5753, https://doi.org/10.1016/j.electacta.2006.03.008.
[16] J. Zhang, B.A. Litteer, W. Gu, H. Liu, H.A. Gasteiger, Effect of hydrogen and oxygen partial pressure on Pt precipitation within the membrane of PEMFCs, J. Electrochem. Soc. 154 (2007) B1006–B1011, https://doi.org/10.1149/1.2764240.
[17] M. Danilczuk, F.D. Coms, S. Schlick, Visualizing chemical reactions and crossover processes in a fuel cell inserted in the ESR resonator: detection by spin trapping of oxygen radicals, nafion-derived fragments, and hydrogen and deuterium atoms, J. Phys. Chem. B 113 (2009) 8031–8042, https://doi.org/10.1021/jp901597f.
[18] A. Ohma, S. Suga, S. Yamamoto, K. Shinohara, Membrane degradation behavior during open-circuit voltage hold test, J. Electrochem. Soc. 154 (2007) B757–B760, https://doi.org/10.1149/1.2741129.
[19] J. Miyake, T. Watanabe, H. Shintani, Y. Sugawara, M. Uchida, K. Miyatake, Reinforced polyphenylene ionomer membranes exhibiting high fuel cell performance and mechanical durability, ACS Mater. Au 1 (2021) 81–88, https://doi.org/10.1021/acsmaterialsau.1c00002.
[20] T. Holmes, T.J.G. Skalski, M. Adamski, S. Holdcroft, Stability of hydrocarbon fuel cell membranes: reaction of hydroxyl radicals with sulfonated phenylated polyphenylenes, Chem. Mater. 31 (2019) 1441–1449, https://doi.org/10.1021/acs.chemmater.8b05302.
[21] C. Lim, A.S. Alavijeh, M. Lauritzen, J. Kolodziej, S. Knights, E. Kjeang, Fuel cell durability enhancement with cerium oxide under combined chemical and mechanical membrane degradation, ECS Electrochem. Lett. 4 (2015) F29–F31, https://doi.org/10.1149/2.0081504eel.
[22] B.P. Pearman, N. Mohajeri, R.P. Brooker, M.P. Rodgers, D.K. Slattery, M. D. Hampton, D.A. Cullen, S. Seal, The degradation mitigation effect of cerium oxide in polymer electrolyte membranes in extended fuel cell durability tests, J. Power Sources 225 (2013) 75–83, https://doi.org/10.1016/j.jpowsour.2012.10.015.
[23] Z.A.R. Gautama, Y.A. Hutapea, B. Hwang, J. Matsuda, A. Mufundirwa, T. Sugiyama, M. Ariyoshi, S. Fujikawa, S.M. Lyth, A. Hayashi, K. Sasaki, M. Nishihara, Suppression of radical attack in polymer electrolyte membranes using a vinyl polymer blend interlayer with low oxygen permeability, J. Membr. Sci. 658 (2022) 120734, https://doi.org/10.1016/j.memsci.2022.120734.
[24] A. Dufresne, Nanocellulose processing properties and potential applications, Curr. For. Reports 5 (2019) 76–89, https://doi.org/10.1007/s40725-019-00088-1.
[25] T. Bayer, B.V. Cunning, R. Selyanchyn, M. Nishihara, S. Fujikawa, K. Sasaki, S. M. Lyth, High temperature proton conduction in nanocellulose membranes: paper fuel cells, Chem. Mater. 28 (2016) 4805–4814, https://doi.org/10.1021/acs.chemmater.6b01990.
[26] O. Selyanchyn, R. Selyanchyn, S.M. Lyth, A review of proton conductivity in cellulosic materials, Front. Energy Res. 8 (2020) 596164, https://doi.org/10.3389/fenrg.2020.596164.
[27] T. Saito, Y. Matsuo, K. Tabata, T. Makino, T. Nohara A. Masuhara, Highly proton conductive membranes based on poly(vinylphosphonic acid)-coated cellulose nanocrystals and cellulose nanofibers for polymer electrolyte fuel cells, Energy Fuels 38 (5) (2024) 4645–4652, https://doi.org/10.1021/acs.energyfuels.3c04336.
[28] T. Bayer, B.V. Cunning, B. Šmíd, R. Selyanchyn, S. Fujikawa, K. Sasaki, S.M. Lyth, Spray deposition of sulfonated cellulose nanofibers as electrolyte membranes in fuel cells, Cellulose 28 (2021) 1355–1367, https://doi.org/10.1007/s10570-020-03593-w.
[29] O. Selyanchyn, T. Bayer, D. Klotz, R. Selyanchyn, S.M. Lyth, Cellulose nanocrystals crosslinked with sulfosuccinic acid as sustainable proton exchange membranes for electrochemical energy applications, Membranes 12 (2022) 658, https://doi.org/10.3390/membranes12070658.
[30] T. Bayer, S.R. Bishop, M. Nishihara, K. Sasaki, S.M. Lyth, Characterization of a graphene oxide membrane fuel cell, J. Power Sources 272 (2014) 239–247, https://doi.org/10.1016/j.jpowsour.2014.08.071.
[31] T. Bayer, B.V. Cunning, R. Selyanchyn, T. Daio, M. Nishihara, S. Fujikawa, K. Sasaki, S.M. Lyth, Alkaline anion exchange membranes based on KOH-treated multilayer graphene oxide, J. Membr. Sci. 508 (2016) 51–61, https://doi.org/10.1016/j.memsci.2016.02.017.
[32] T. Bayer, R. Selyanchyn, S. Fujikawa, K. Sasaki, S.M. Lyth, Spray-painted graphene oxide membrane fuel cells, J. Membr. Sci. 541 (2017) 347–357, https://doi.org/10.1016/j.memsci.2017.07.012/.
[33] M. Breitwieser, T. Bayer, A. Büchler, R. Zengerle, S.M. Lyth, S. Thiele, A fully spray-coated fuel cell membrane electrode assembly using Aquivion ionomer with

a graphene oxide/cerium oxide interlayer, J. Power Sources 351 (2017) 145–150, https://doi.org/10.1016/j.jpowsour.2017.03.085.
[34] M.J. Choo, K.H. Oh, H. Park, J.K. Park, New cross-linked interfacial layer on hydrocarbon membrane to improve long-term stability of polymer electrolyte fuel cells, Electrochim. Acta 92 (2013) 285–290, https://doi.org/10.1016/j.electacta.2013.01.038.
[35] R.R. Raja Rafidah, W. Rashmi, M. Khalid, W.Y. Wong, J. Priyanka, Recent progress in the development of aromatic polymer-based proton exchange membranes for fuel cell applications, Polymers 12 (2020) 1061, https://doi.org/10.3390/polym12051061.
[36] M. Rahaman, A. Aldalbahi, P. Govindasami, N.P. Khanam, S. Bhandari, P. Feng, T. Altalhi, A new insight in determining the percolation threshold of electrical conductivity for extrinsically conducting polymer composites through different sigmoidal models, Polymers 9 (10) (2017) 527, https://doi.org/10.3390/polym9100527.
[37] A. Redondo, N. Mortensen, K. Djeghdi, D. Jang, R.D. Ortuso, C. Weder, L.T. J. Korley, U. Steiner, I. Gunkel, Comparing percolation and alignment of cellulose nanocrystals for the reinforcement of polyurethane nanocomposites, ACS Appl. Mater. Interfaces 14 (2022) 7270–7282, https://doi.org/10.1021/acsami.1c21656.
[38] H. Wang, H. Du, K. Liu, H. Liu, T. Xu, S. Zhang, X. Chen, R. Zhang, H. Li, H. Xie, X. Zhang, C. Si, Sustainable preparation of bifunctional cellulose nanocrystals via mixed H2SO4/formic acid hydrolysis, Carbohydr. Polym. 266 (2021) 118107, https://doi.org/10.1016/j.carbpol.2021.118107.
[39] H. Wang, H. Xie, H. Du, X. Wang, W. Liu, Y. Duan, X. Zhang, L. Sun, X. Zhang, C. Si, Highly efficient preparation of functional and thermostable cellulose nanocrystals via H2SO4 intensified acetic acid hydrolysis, Carbohydr. Polym. 239 (2020) 116233, https://doi.org/10.1016/j.carbpol.2020.116233.
[40] T. Saito, Y. Matsuo, K. Tabata, T. Makino, T. Nohara, A. Masuhara, Highly proton conductive membranes based on poly(vinylphosphonic acid)-coated cellulose nanocrystals and cellulose nanofibers for polymer electrolyte fuel cells, Energy Fuels 38 (2024) 4645–4652, https://doi.org/10.1021/acs.energyfuels.3c04336.
[41] M. Ludvigsson, J. Lindgren, J. Tegenfeldt, Crystallinity in cast nafion, J. Electrochem. Soc. 147 (2000) 1303, https://doi.org/10.1149/1.1393354.
[42] J. Gong, J. Li, J. Xu, Z. Xiang, L. Mo, Research on cellulose nanocrystals produced from cellulose sources with various polymorphs, RSC Adv. 7 (2017) 33486–33493, https://doi.org/10.1039/C7RA06222B.
[43] M.K. Mohanapriya, K. Deshmukh, K. Chidambaram, M.B. Ahamed, K. K. Sadasivuni, D. Ponnamma, M.A.-A. AlMaadeed, R.R. Deshmukh, S.K.K. Pasha, Polyvinyl alcohol (PVA)/polystyrene sulfonic acid (PSSA)/carbon black nanocomposite for flexible energy storage device applications, J. Mater. Sci. Mater. Electron. 28 (2017) 6099–6111, https://doi.org/10.1007/s10854-016-6287-2.
[44] P.C. van derHeijden, L. Rubatat, O. Diat, Orientation of drawn nafion at molecular and mesoscopic scales, Macromolecules 37 (2004) 5327–5336, https://doi.org/10.1021/ma035642w.
[45] K.A. Page, F.A. Landis, A.K. Phillips, R.B. Moore, SAXS analysis of the thermal relaxation of anisotropic morphologies in oriented nafion membranes, Macromolecules 39 (2006) 3939–3946, https://doi.org/10.1021/ma052359j.
[46] E.E. Ureña-Benavides, C.L. Kitchens, Wide-angle X-ray diffraction of cellulose Nanocrystal−Alginate nanocomposite fibers, Macromolecules 44 (2011) 3478–3484, https://doi.org/10.1021/ma102731m.
[47] X. Ju, M. Bowden, E.E. Brown, X. Zhang, An improved X-ray diffraction method for cellulose crystallinity measurement, Carbohydr. Polym. 123 (2015) 476–481, https://doi.org/10.1016/j.carbpol.2014.12.071.
[48] G. Delepierre, S. Eyley, W. Thielemans, C. Weder, E.D. Cranston, J.O. Zoppe, Patience is a virtue: self-assembly and physico-chemical properties of cellulose nanocrystal allomorphs, Nanoscale 12 (2020) 17480–17493, https://doi.org/10.1039/D0NR04491A.
[49] X. Cheng, Z. Shi, N. Glass, L. Zhang, J. Zhang, D. Song, Z.-S. Liu, H. Wang, J. Shen, A review of PEM hydrogen fuel cell contamination: impacts, mechanisms, and mitigation, J. Power Sources 165 (2007) 739–756, https://doi.org/10.1016/j.jpowsour.2006.12.012.
[50] E.R.G. Thiago Lopes, Valdecir A. Paganin, The effects of hydrogen sulfide on the polymer electrolyte membrane fuel cell anode catalyst: H2S–Pt/C interaction products, J. Power Sources 196 (2011) 6256–6263, https://doi.org/10.1016/j.jpowsour.2011.04.017.
[51] S.D. Mikhailenko, G.P. Robertson, M.D. Guiver, S. Kaliaguine, Properties of PEMs based on cross-linked sulfonated poly(ether ether ketone), J. Membr. Sci. 285 (2006) 306–316, https://doi.org/10.1016/j.memsci.2006.08.036.
[52] K.J. De France, T. Hoare, E.D. Cranston, Review of hydrogels and aerogels containing nanocellulose, Chem. Mater. 29 (2017) 4609–4631, https://doi.org/10.1021/acs.chemmater.7b00531.
[53] D. Trache, M.H. Hussin, M.K.M. Haafiz, V.K. Thakur, Recent progress in cellulose nanocrystals: sources and production, Nanoscale 9 (2017) 1763–1786, https://doi.org/10.1039/C6NR09494E.
[54] M.S. Reid, M. Villalobos, E.D. Cranston, Benchmarking cellulose nanocrystals: from the laboratory to industrial production, Langmuir 33 (7) (2017) 1583–1598, https://doi.org/10.1021/acs.langmuir.6b03765.
[55] S.H. Shin, A. Kodir, D. Shin, S.H. Park, B. Bae, Perfluorinated composite membranes with organic antioxidants for chemically durable fuel cells, J. Electrochimica Acta 298 (2019) 901–909, https://doi.org/10.1016/j.electacta.2018.12.150.
[56] Y. Oshiba, M. Kosaka, T. Yamaguchi, Chemical durability of thin pore-filling membrane in open-circuit voltage hold test, J. Int. J. Hydrogen Energy 44 (54) (2019) 28996–29001, https://doi.org/10.1016/j.ijhydene.2019.09.143.